

Block Copolymer-Assembled Nanopores Enable Ultra-Sensitive Label-Free DNA Detection

*Maximiliano Jesus Jara Fornerod^a, Alberto Alvarez-Fernandez^a, Mate Furedi^a,
Anandapadmanabhan A Rajendran^b, Beatriz Prieto-Simon^{c,d}, Nicolas H. Voelcker^{e,f,*}, Stefan
Guldin^{a,*}*

^aDepartment of Chemical Engineering, University College London, Torrington Place, London,
WC1E 7JE, UK.

^bDepartment of Electronic Engineering, Universitat Rovira i Virgili, 43007, Tarragona, Spain

^cInstitute of Chemical Research of Catalonia, The Barcelona Institute of Science and
Technology, Av. Països Catalans, 16, 43007, Tarragona, Spain

^dICREA, Pg. Lluís Companys 23, 08010, Barcelona, Spain

^eMonash Institute of Pharmaceutical Sciences, Monash University, Parkville, Victoria, 3052,
Australia

^fMelbourne Centre for Nanofabrication, Victorian Node of the Australian National Fabrication
Facility, Clayton, Victoria, 3168, Australia

*corresponding authors. E-mail address: nicolas.voelcker@monash.edu, s.guldin@ucl.ac.uk

Keywords: DNA detection; electrochemical biosensor; nanoporous; block copolymer; sol-gel

Abstract

DNA detection plays an important role in pathogen identification and disease diagnosis but is often limited by lengthy processing times, high costs, and the need for complex equipment and skilled personnel, making it less accessible in point-of-care and resource-limited environments. In this study, we introduce an electrode modification strategy for DNA detection that uses block copolymer-directed nanoporous thin films for nanopore blockage (NB)-based electrochemical biosensors. This approach enables rapid, label-free DNA detection and quantification at femtomolar levels. Deploying a bottom-up fabrication process that leverages on the self-assembly of high molecular weight block copolymers with inorganic sol-gel precursors, we create a highly scalable nanoporous thin film architecture with tailored pore size and arrangement. Crucially, we eliminate the need for complex fabrication including stacking brittle porous membranes, a constraint in existing NB-based DNA sensors. The rapid performance of this sensor is demonstrated by detecting specific single-stranded DNA sequences derived from the 16S rRNA gene fragment of the *E. coli* genome within 20 minutes, achieving a limit of detection of 30 fM and a limit of quantification of 500 fM. The development of this DNA biosensor represents a significant advancement towards a portable, user-friendly, rapid, cost-effective, and highly accurate DNA detection platform, promising to overcome current limitations of conventional detection methods and broadening the applicability of DNA diagnostics across diverse use cases.

Introduction

DNA detection is essential for identifying pathogens, including viruses and bacteria, and in diagnosing a range of diseases.¹ Its importance was highlighted during the COVID-19 pandemic, where it was critical in disease management because it facilitated the identification of infected individuals, thus helping to slow the spread of the disease. DNA detection extends to the diagnosis of non-infectious conditions, such as identifying mutations in circulating cell-free DNA through

liquid biopsies or detecting the overexpression of oncogenes in conventional biopsies.^{2,3} Beyond diagnostics, DNA detection finds applications in diverse fields including water treatment evaluation,⁴ environmental and agricultural monitoring,⁵ and biological weapon detection.⁶ From an analytical perspective, polymerase chain reaction (PCR) stands as the gold standard in DNA detection.^{7,8} However, its universal adoption is hindered by time-consuming procedures, the requirement for trained personnel, high materials costs, and the lack of portable equipment.^{9–11}

Electrochemical DNA detection offers a compelling alternative to PCR, providing rapid, cost-effective, and labor-free sample preparation with quantitative readouts.¹² Recent advancements in electrode modification using nanoporous materials have significantly enhanced sensitivity and stability, while reducing the matrix effect in electrochemical (bio)sensors.^{13–16} A major innovation in this field is the use of a nanoporous membrane on top of the electrode, enabling a detection method based on the nanopore blockage (NB) caused upon DNA hybridization.^{17–20} This method relies on variations in the electrochemical signal that occur when target nucleic acids hybridize to their complementary strand inside a nanoscale pore, resulting in pore blockage and a quantitative response that correlates with the concentration of the target analyte.^{17,19,21} Furthermore, tailoring the nanopores size for the target analyte also enhances sensor selectivity by preventing the entry of larger, non-target molecules into the nanopores.^{22,23}

Despite notable progress, challenges persist in the production of NB-based DNA sensors. Currently, fabricating these sensors involves mechanically attaching a nanoporous membrane onto a conductive substrate that serves as the electrode. Traditionally, porous silicon (pSi) and nanoporous anodic alumina (NAA) produced via electrochemical anodization, have been deployed as the nanoporous layer.^{13,24} However, the inherent fragility of these materials and the complex assembly process of the membrane have limited the application of these DNA sensors beyond

research laboratories.²⁵ Additionally, the production of nanoporous membranes from silicon wafers involves the use of hydrofluoric acid (HF),¹⁴ a highly toxic substance, while aluminum processing can lead to the formation of potentially explosive by-products.¹³ In light of these challenges, there is an urgent need to develop innovative methods that enable seamless integration of nanoporous electrode architectures for DNA detection.^{16,26}

A promising alternative for producing the nanoporous layer involves using block copolymers (BCPs) micelles as sacrificial templates for sol-gel materials. This method offers the capability to create inorganic nanopores across the entire mesoporous range (i.e. 2 to 50 nm) by using BCPs with varying molecular weights,²⁷ and is compatible with a broad spectrum of sol-gel materials.^{28,29} Fine-tuning of nanopore size and porosity is achievable through various processing methods such as solvent vapor annealing,³⁰ homopolymer swelling,^{31,32} or chromatographic fractionation of BCPs.³³ The high level of structural control offered by this fabrication method, along with the ability to directly process this nanomaterial onto the electrode surface without the need for stacking a membrane, holds significant promise for DNA detection. However, the use of sol-gel materials and BCPs in NB-based biosensors remains largely unexplored, mainly due to challenges related to film shrinkage during processing, especially at high block copolymer concentrations, as well as tailored surface functionalization, interfacial reconstruction, and segregation of the sol-gel avoiding continuous pore access towards the bottom electrode.^{34,35}

In this work, we report the development of a DNA biosensor based on the NB effect that employs a block copolymer-templated nanoporous thin film as support of the biorecognition layer. We achieved rapid, label-free, and quantitative detection of DNA at femtomolar levels by measuring impedimetric changes resulting from hybridization between single-stranded DNA (ssDNA) capture probes immobilized on the nanopore walls with a target ssDNA sequences, corresponding

to an *E. coli* genome 16S ribosomal RNA gene fragment (**Figure 1**). Characterization of the nanoarchitectures was conducted using various analytical techniques, including spectroscopic ellipsometry, ellipsometric porosimetry, scanning electron microscopy (SEM), focused ion beam (FIB) microscopy, atomic force microscopy (AFM), and grazing incidence small-angle X-ray scattering (GISAXS). Additionally, quartz crystal microbalance with dissipation monitoring (QCM-D) enabled to study the efficiency of the functionalization of the nanopores with ssDNA capture probes, and to determine the time required for efficient hybridization.

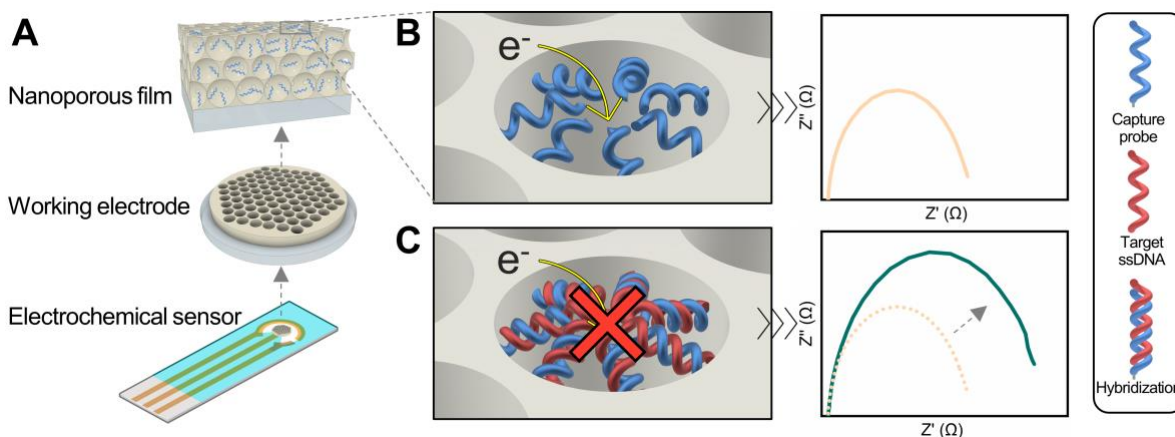


Figure 1. Schematic of the electrochemical DNA detection. A) The working electrode of a 3-electrode electrochemical biosensor is coated with a block copolymer-derived nanoporous layer and functionalized with ssDNA capture probes designed for selective hybridization of target DNA sequences. B) Prior to sample exposure, the baseline electrochemical impedance is measured. C) Hybridization of the DNA sequence in the liquid sample to its matching ssDNA probe on the biosensor results in blocking of the nanopore and an increase in the impedance signal that can be deployed for quantification.

Results and discussion

Synthesis of inorganic nanoporous films directed by block copolymers

We used the BCP poly(isoprene)-block-poly(ethylene oxide) (PI-*b*-PEO) as a structural guide for assembling aluminosilicate sol-gel into a nanoporous architecture, as depicted in **Figure 2a**. The initial step involved dissolving PI-*b*-PEO in a selective solvent to induce the self-assembly of the BCP into micelles, and subsequently adding the aluminosilicate sol-gel to co-assemble with the PEO block. This mixture was then spin-coated onto an FTO-coated glass substrate that serves as electrode. The resultant thin film was calcined in two steps: first under argon to condense the sol-gel around the BCP micelles, and then in air to remove the carbonized BCP, revealing the pores.³⁴ We used a high BCP concentration in the mixture to generate nanopores with both high porosity and large pore sizes, aiming to facilitate the diffusion of ssDNA within the nanoporous film.^{36,37} The initial calcination step in argon was found in preceding studies to be crucial for mitigating fabrication issues associated with the high BCP content, i.e. minimizing uniaxial shrinkage of the sol-gel and preventing collapse of the nanostructure.³⁴

We determined the film thickness through spectroscopic ellipsometry (SE) and characterized the accessible porosity, pore dimensions, and surface area via ellipsometric porosimetry (EP). A film thickness of approximately 150 nm and a refractive index of 1.12 was derived from fitting the ellipsometric angles ψ and Δ using a Cauchy dispersion law (**Figure 2b**). The EP isotherms (dashed line in **Figure 2c**) revealed an accessible porosity of 65%. Moreover, the type IV with H2(b) hysteresis loop isotherm suggests the interconnection of the nanopores via pore necks.³⁸ Applying the modified Kelvin equation on the EP isotherms (**Figure 2d**) provided pore size and pore neck size distributions of 44 ± 12 nm and 23 ± 11 nm, respectively.³⁹ Additionally, a surface area of $140\text{ m}^2\text{cm}^{-3}$ was calculated using the Brunauer–Emmett–Teller (BET) method.⁴⁰

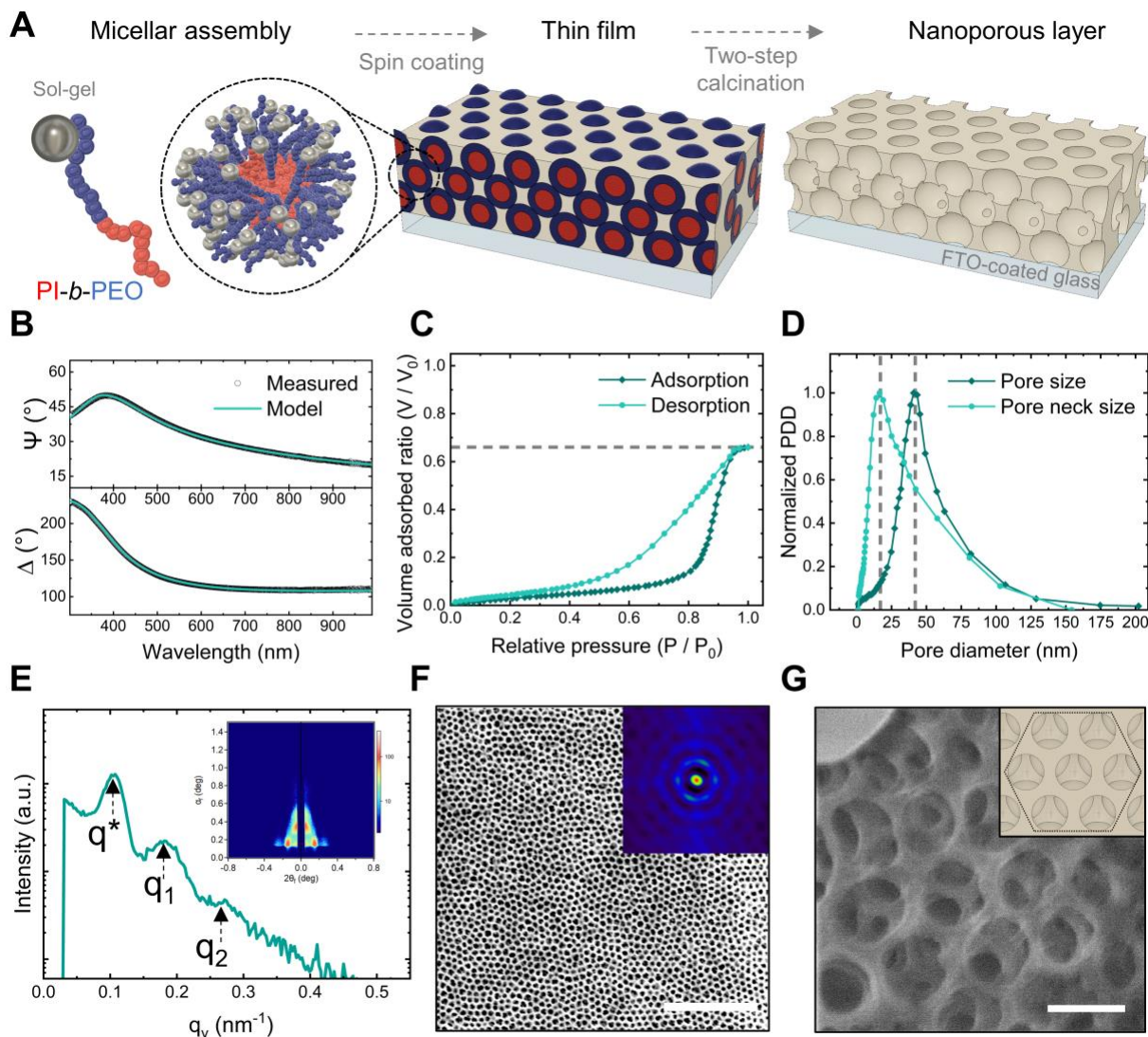


Figure 2. **Nanoporous architecture.** A) Schematic of the fabrication process via BCP self-assembly. B) Measured and modelled ellipsometric angles ψ and Δ for film thickness and refractive index determination. C) Ellipsometric porosimetry isotherms using toluene as adsorptive. D) Pore size distribution derived from the EP isotherms. E) 2D GISAXS scattering pattern of the nanoporous film. F) SEM image of a nanoporous thin film with the 2D spatial distribution function (inset) to evaluate pore ordering. Scale bar: 1 μm . G) High magnification FIB image showing the nanopores and pore necks alongside a schematic top view of a perfect hexagonal close-packed pore configuration in the inset (FIB image scale bar: 100 nm).

To investigate the spatial arrangement of the nanopores, we obtained grazing incidence small-angle X-ray scattering (GISAXS) patterns of the film and high magnification images of the films' surface. The observation of numerous Bragg peaks in the in-plane line-cuts integration of GISAXS patterns (**Figure 2e**) revealed evidence of a long-range porous ordering, with the first Bragg peak ($q^*=0.102\text{ nm}^{-1}$) and higher order peaks q_1 and q_2 consistent with the formation of various symmetric arrangements.^{41,42} The SEM micrograph analysis, by means of a 2D spatial distribution function (inset in **Figure 2f**), showed concentric hexagonal rings, indicating a degree of hexagonal close-packed (HCP) order on the nanoporous surface. Additionally, a high magnification focused ion beam (FIB) micrograph (**Figure 2g**) confirmed that the surface pores were interconnected with the underlying pores through smaller necks. Alongside, cross-sectional SEM (see micrograph in Supporting Information **Figure S1**) supported the thickness measurements obtained via SE.

This nanoarchitecture is a good candidate for NB-based DNA biosensors for several reasons. Firstly, its large surface area enables the immobilization of a high density of ssDNA capture probes, thereby increasing the probability and dynamic range for capturing the target DNA molecules. Secondly, the film's thickness is an order of magnitude thinner than that of previously reported NB-sensors.⁴³ Prior research indicates that thinner membranes are more effective than thicker ones, as lengthy nanochannels can hinder electrolyte diffusion, leading to increased electrical resistance and reduced sensitivity.^{43,44} Thirdly, the size of the pore necks closely matches that of typical ssDNA capture probes (30 to 40 base pairs in length, equivalent to 10 to 13 nm), potentially enhancing pore-blocking efficiency by aligning the pore diameter with the target molecule size.⁴⁴ Finally, we want to highlight that previous NB-based electrochemical biosensors predominantly utilized materials with vertically oriented cylindrical nanopores. The use of a block copolymer-derived inverse opal-type architecture with highly uniform pore and neck sizes has not been

reported yet. We hypothesize that the restrictions created by the pore necks could favor pore blocking compared to other configurations and that the multiple percolation paths across the architecture may enhance the dynamic range. **Table 1** summarizes the structural parameters of the nanoporous architecture.

Table 1: Structural parameters of the nanostructure.

Film thickness [nm]	Porosity [vol%]	Mean pore size D_{ads} [nm]	Mean pore neck size D_{des} [nm]	Surface area [m^2cm^{-3}]
150	65	44±12	23±10.5	140

Surface functionalization with single-stranded DNA capture probes

We functionalized the nanopore walls with ssDNA capture probes to act as the biorecognition element for targeting specific ssDNA sequences.⁴⁸ The functionalization process involved the sequential use of amino-silane (APTES) and glutaraldehyde (GA) for the immobilization of an amino-modified ssDNA (ssDNA-NH₂) onto plasma-activated nanopore walls.⁴⁹ Ethanolamine was subsequently applied as a blocking agent of unreacted aldehyde groups. **Figure 3a** schematizes the functionalization protocol.

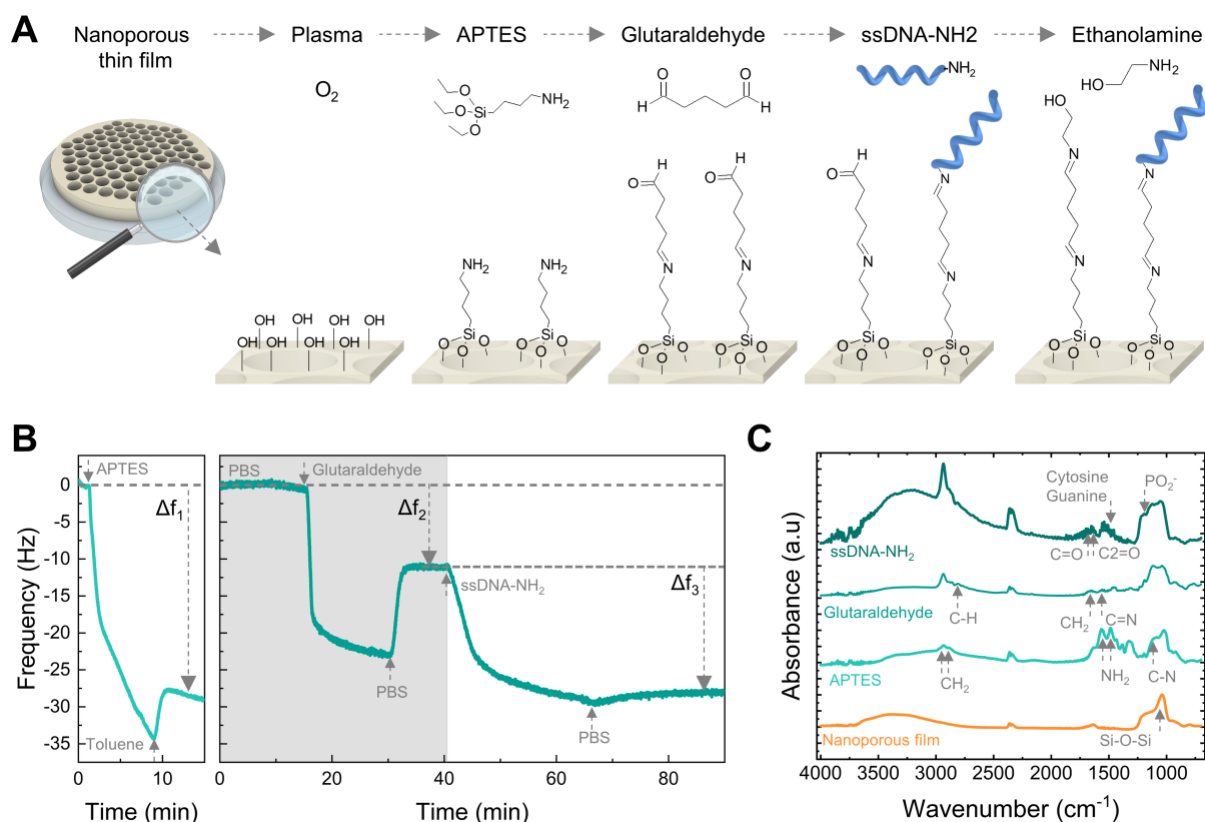


Figure 3 Surface modification with nucleic acid capture probes. A) Schematic of the surface functionalization with ssDNA. B) Real-time surface functionalization measurements using QCM-D sensors. Frequency response (5th harmonic) of a sensor coated with a nanoporous film during surface modification in toluene (left) and PBS buffer (right), respectively. C) FTIR spectra of a nanoporous film during the sequential surface modification with APTES, glutaraldehyde, and amino-modified ssDNA.

We used a quartz crystal microbalance with dissipation monitoring (QCM-D) to study the surface modification protocol in real-time. **Figure 3b** shows the frequency shifts of the fifth harmonic of a QCM-D sensor coated with the nanoporous film during modification with APTES (left) and subsequently with GA and ssDNA-NH₂ (right). In QCM-D measurements, a decrease in frequency is consistent with mass adsorption at the sensor interface, while frequency increase indicates mass

release.⁵⁰ The observed negative frequency shifts upon exposure to APTES, GA, and ssDNA are consistent with the immediate adsorption of these molecules onto the sensor surface. Rinsing with the appropriate solvent aids the removal of non-covalently bound molecules. Thus, the net negative frequency changes post-rinse (i.e., Δf_1 , Δf_2 , and Δf_3), observed after each functionalization step, underpin the rapid, stable, and permanent binding of APTES, GA, and ssDNA probes to the surface. We measured the FTIR spectra at each step of the functionalization of the nanoporous surface to confirm the covalent binding (**Figure 3c**). The aluminosilicate matrix was identified by the peak at 1037 cm^{-1} corresponding to the asymmetric stretch of Si-O-Si, consistent with the high silica content. Subsequent aminosilanization led to new peaks at 1550 cm^{-1} and 1485 cm^{-1} attributed to the NH_2 bending of the amine groups,⁵¹ as well as the C-N stretching at 1150 cm^{-1} alongside the CH_2 stretching at 2885 cm^{-1} and 2935 cm^{-1} . Next, the crosslinking with glutaraldehyde produced the loss of the NH_2 bands and the formation of C=N bonds (1652 cm^{-1}).⁵² Additionally, the peaks at 1450 cm^{-1} and 2812 cm^{-1} correspond to the CH_2 deformation and C-H stretching of the aldehyde groups. Attachment of the ssDNA probes produced a peak at 1225 cm^{-1} , attributed to the PO_2^- asymmetric stretching of phosphate groups.⁵³ Furthermore, DNA base-specific peaks were identified: the peak at 1527 cm^{-1} for the in-plane vibration of cytosine and guanine DNA bases, while the peaks at 1661 cm^{-1} and 1710 cm^{-1} correlated with the C=N stretching in thymine bases and the C=O stretching of guanine groups, respectively.⁵³

Additionally, we also verified that ssDNA capture probes were anchored not only on the surface but also within the nanoporous structure by employing ssDNA- NH_2 modified with the fluorescent molecule cyanine-5 (Cy5) (see Supporting Information, **Figure S2**). The fluorescence intensity of ssDNA functionalized on the nanopore-coated surface was fourteen times greater than that of a

flat QCM-D sensor used for reference, confirming that ssDNA was immobilized inside the nanopores and taking advantage of the high surface area available for attachment.

Electrochemical detection of single-stranded DNA through nanoporous blockage (NB)

To investigate the use of this material platform for NB-based DNA detection, we employed a 28-base nucleic acid sequence specific to *Escherichia coli* (*E.coli*) derived from 16S ribosomal RNA gene as the target ssDNA.⁵⁴ In our sensing approach, we used its complementary ssDNA immobilized within the nanopores as a positive control, alongside a non-complementary ssDNA serving as a negative control, as schematically shown in **Figure 4a**.

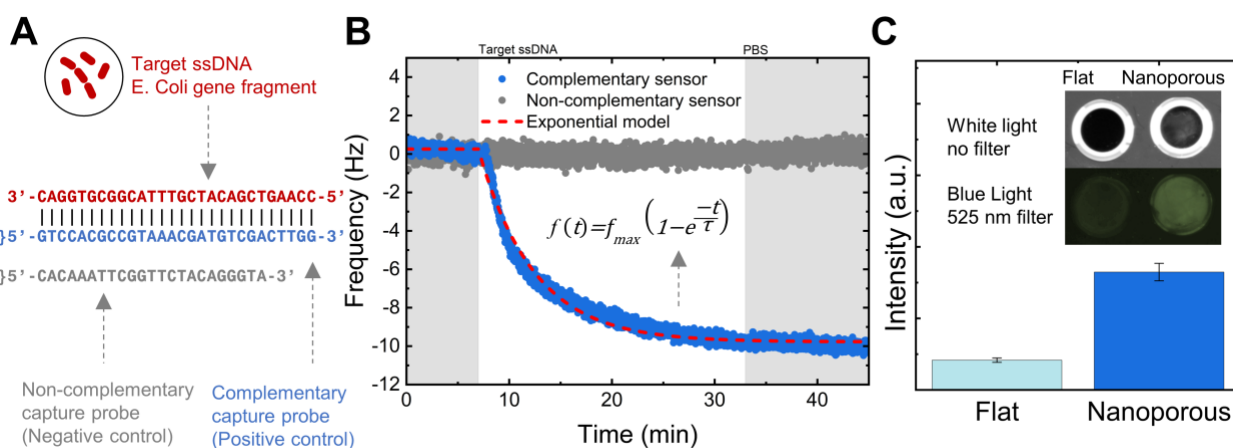


Figure 4 DNA hybridization in the nanoporous layer. A) DNA sequences of the target and capture probes used for sensing. B) Frequency changes of nanoporous-coated QCM-D sensors functionalized with complementary and non-complementary capture probes upon exposure to the target ssDNA. B) Comparative fluorescence intensity between a nanoporous-coated and a flat QCM-D sensors hybridized with a target ssDNA modified with the fluorescent molecule (6FAM) (exposure time: 30s). The inset shows the QCM-D sensors.

We determined the time required for nucleic acid detection assays by monitoring the frequency changes in nanoporous-coated QCM-D sensors functionalized with the capture probes upon exposure to the target ssDNA, as depicted in **Figure 4b**. The frequency variation over time observed in the nanoporous-coated QCM-D sensor functionalized with the complementary capture probe demonstrated the rapid hybridization with the target ssDNA. Conversely, the non-complementary sensor exhibited no lasting frequency changes. We used an exponential association equation to model the frequency changes produced by the target ssDNA with its complementary capture probe:

$$f(t) = f_{max} \left(1 - e^{-\frac{t}{\tau}}\right), \quad (1)$$

where $f(t)$ represents the frequency change at any given time (t), with a time constant $\tau = 5.36 \pm 0.63$ min (average of three measurements) and f_{max} being the maximum frequency change at equilibrium. We established that the optimal time for nucleic acid detection assays is three times the time constant τ . This duration represents a balanced compromise between the time necessary for sensing and achieving near equilibrium hybridization (i.e. >95%), as we show in the Supporting Information.

To measure the DNA hybridization efficiency in the nanoporous layer, we used a target ssDNA modified with the fluorescent molecule 6-carboxyfluorescein (6-FAM) and compared the fluorescence intensity between a nanoporous-coated and a flat QCM-D sensor, both functionalized with the complementary ssDNA capture probe (**Figure 4c**). The fluorescence intensity of the nanoporous-coated QCM-D sensor was found to be four times greater than that of the flat sensor. This contrasts with the fluorescence intensity previously measured for the capture probes alone, which were more than ten-fold higher on the nanoporous surface compared to the flat sensor. This

difference suggests that hybridization predominantly occurs on the surface of the nanoporous layer, effectively blocking access to the underlying nanopores.

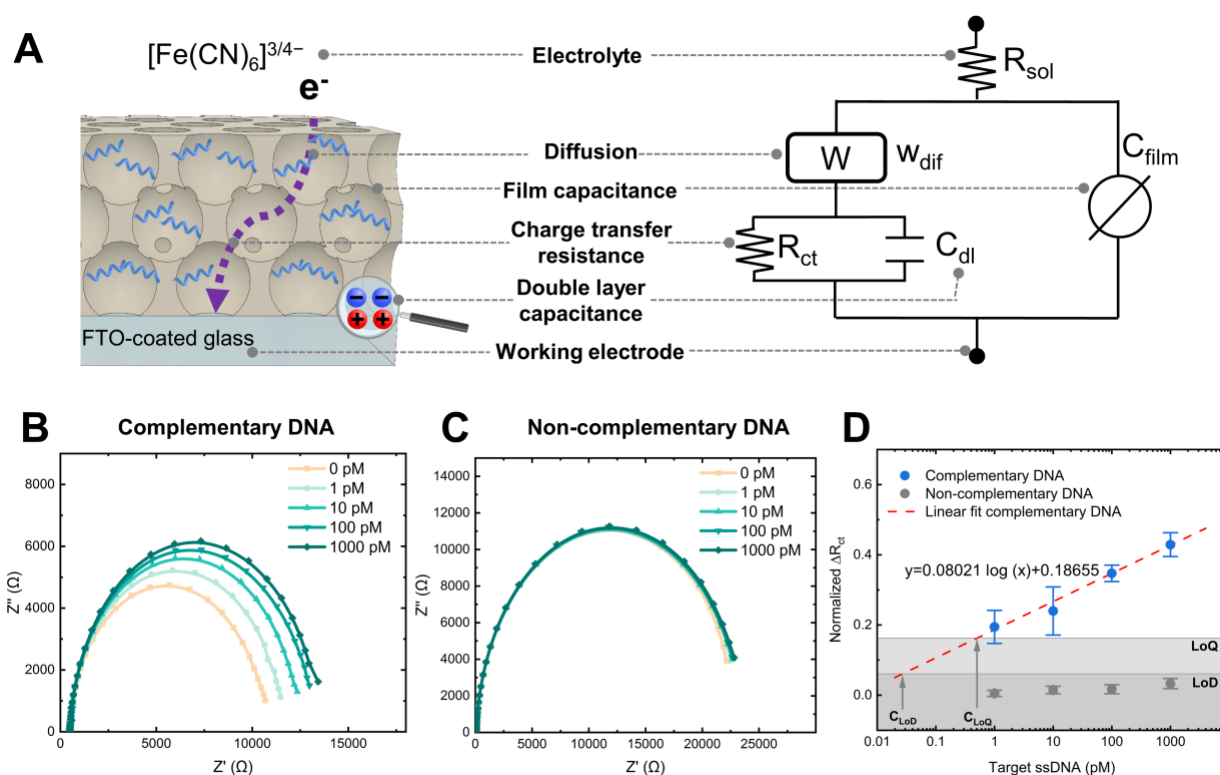


Figure 5. **Electrochemical detection of DNA.** A) Schematic and corresponding equivalent circuit of the nanoporous sensor used to interpret impedimetric measurements. B) Nyquist plots of a complementary sensor (positive control) upon exposure to different concentrations of the target ssDNA. C) Nyquist plots of a non-complementary sensor (negative control) upon exposure to different concentrations of the target ssDNA. D) Concentration-response curves of the nanoporous sensors (complementary and non-complementary), error bars correspond to the standard deviation of at least three sensors.

We detected the target DNA electrochemically using a three-electrode setup, comprising the FTO-coated glass modified with the nanoporous layer as the working electrode, a platinum wire as the counter electrode, and a silver/silver chloride reference electrode. The redox mediator

ferricyanide/ferrocyanide was chosen based on evidence from previous studies that the blocking effect upon DNA hybridization is enhanced with a negatively charged redox probe.^{19,20} See Supporting Information **Figure S3** for a schematic of the setup.

We measured electrochemical impedance spectroscopy (EIS) to monitor changes in the electrical resistance of the system due to nanoporous blockage. An equivalent circuit model of the nanoporous sensor was used to determine changes in electrical resistance from the measured impedance (**Figure 5a**).⁵⁵ This model included the charge transfer resistance (R_{ct}), double-layer capacitance at the electrode interface (C_{dl}), a Warburg element for diffusion in the film (W_{dif}), the nanoporous film's capacitance modelled as a constant phase element (C_{film}), and the solution resistance (R_{sol}).

Nyquist plots of sensors functionalized with the complementary ssDNA showed distinctive impedance increases upon incubation with target ssDNA, from 1 pM to 1 nM concentrations (**Figure 5b**). In contrast, sensors with the non-complementary ssDNA capture probe showed negligible impedance changes (**Figure 5c**), proving that the blockage of the nanopores produced the changes in impedance and demonstrating the specificity of the sensor.

We normalized the R_{ct} values to compare the response between different biosensors (**Figure 5d**). The R_{ct} of complementary sensors increased in proportion to the concentration of the target ssDNA, as shown by the linear fit in **Figure 5d**. The limit of detection (LoD) is the ability to differentiate a positive result from the noise of a blank measurement.⁵⁶ Thus, a LoD of 30 fM was determined using the mean value of the negative control considering three times its standard deviation, along with the linear fit of the positive control. This LoD represents an improvement of one order of magnitude compared to recent works using carbon-stabilized porous silicon films.^{43,57} Similarly, the limit of quantification (LoQ) is the minimum amount of the target analyte that can be quantified

with acceptable precision.⁵⁸ A LoQ of 500 fM was calculated using the average of the negative control increased by ten times its standard deviation,⁵⁹ and the linear fit of the positive control. Please refer to the Supporting Information for equations used in normalizing the R_{ct} and calculating the LoD and LoQ.

The direct fabrication of this nanomaterial onto the working electrode avoids the complex assembly process typical of NB-based biosensors. This advancement, coupled with the successful detection of nucleic acids with an improved LoD compared to previous generations of NB-based biosensors, and the potential for scale-up of the fabrication process, allows envisioning its integration into a test strip for rapid nucleic acid detection similar to those commonly employed for glucose monitoring. Crucially, the capability for quantification extends the relevance of this platform to scenarios requiring the measurement of nucleic acid concentrations. Further improvements in LoDs could be achieved through integration with isothermal nucleic acid amplification techniques, such as loop-mediated isothermal amplification (LAMP) or rolling circle amplification (RCA).⁶⁰ Finally, while the biosensor initially targeted DNA due to its stability and cost-effectiveness compared to RNA, it retains the capability to detect RNA without requiring additional modifications. Direct RNA detection is practical with our current setup since the ssDNA capture probes we used can also hybridize with complementary RNA sequences. However, it's pertinent to mention that the experiments were performed in a simplified buffer system. Despite this, the ultra-sensitive fM LoD allows for significant dilution of complex biological samples to levels where the expected DNA and RNA concentrations are usually higher, facilitating detection in clinical and environmental contexts. The coming phase of our research will involve direct comparisons using the equivalent RNA sequences in a complex media to fully validate this capability and expand the scope of our sensor's application.

Conclusion

In conclusion, this study introduces a biosensor fabrication approach based on BCP self-assembly for the rapid, quantitative, selective, ultrasensitive, and label-free electrochemical DNA detection via NB. The deployment of a hexagonal close-packed nanoporous structure, with pores approximately 50 nm in diameter and pore necks around 20 nm, enabled the impedimetric detection of target ssDNA with a LoD of 30. Moreover, the linear response of the impedimetric measurements, ranging from 1 pM to 1 nM, allowed for quantification with a LoQ of approximately 500 fM. Remarkably, a 20-minute hybridization time is sufficient to achieve near-equilibrium hybridization of complementary DNA strands, demonstrating its potential for rapid sensing.

Nucleic acid detection is fundamental for various applications, including the detection of viruses, bacteria, and disease markers. Nevertheless, the limitations of conventional nucleic acid detection methods prevent their widespread use. The electrochemical biosensor developed in this study presents a substantial advance towards a portable, easy-to-use, rapid, and inexpensive nucleic acid detection platform, offering a viable alternative to existing detection technologies.

Experimental

Reagents: Poly(1,4-isoprene)-block-poly(ethylene oxide) BCP (polydispersity: 1.01, Mn PI₄₈-b-PEO₁₂ kg mol⁻¹) was obtained from Polymer Source. Toluene (99.9%), toluene (anhydrous, 99.8%), aluminum tri-sec-butoxide (97%), 1-butanol (99.4%), (3-glycidyloxypropyl)-trimethoxysilane (GLYMO) (≥98%), (3-aminopropyl)triethoxysilane (APTES) (99%), potassium chloride (KCl) (≥99.9%), glutaraldehyde solution (Grade I, 25% in H₂O, specially purified for use as an electron microscopy fixative), sodium cyanoborohydride (95%), ethanolamine hydrochloride (≥99.0%), nuclease-free water, and nucleic acids were purchased from Merck. Phosphate buffered

saline (PBS) tablets were obtained from OXOID. The electrolytes potassium ferrocyanide $K_4[Fe(CN)_6]$ (>98.5%) and potassium ferricyanide $K_3[Fe(CN)_6]$ (99+%) were purchased from Honeywell and ACROS Organics, respectively. All chemicals were used as received without further purification. Nucleic acid sequences used for immobilization in the nanoporous structure and sensing are summarized in **Table 2**. NH_2C_6 represents an amine group spaced by six carbons from the DNA bases adenine (A), thymine (T), guanine (G) and cytosine (C). 6FAM and CY5 represent the fluorescent dye modification 6-carboxyfluorescein and cyanine 5, respectively.

Table 2: Nucleic acid sequences used for immobilization and sensing.

5' mod	Nucleic acid sequence 5'to 3'	3' mod	M_w (g mol ⁻¹)	T_m (° C)
NH_2C_6	GTC CAC GCC GTA AAC GAT GTC GAC TTG G		8,769	78.4
NH_2C_6	GTC CAC GCC GTA AAC GAT GTC GAC TTG G	CY5	9,302	78.4
NH_2C_6	CAC AAA TTC GGT TCT ACA GGG TA		7,227	78.4
	CCA AGT CGA CAT CGT TTA CGG CGT GGA C		8,590	63.7
6FAM	CCA AGT CGA CAT CGT TTA CGG CGT GGA C		9,127	78.4

Fabrication of nanoporous aluminosilicate thin films directed by block copolymers: Two stock solutions with fixed concentrations of aluminosilicate and BCP were prepared. First, the aluminosilicate stock solution was made by mixing a silica precursor (2.8 g of GLYMO), an alumina precursor (0.32 g of aluminum tri-sec-butoxide), and 20 mg of KCl in an iced bath. After stirring for 15 min, 135 μ l of 10 mM HCl was added dropwise to the blend, followed by another 15 min of stirring at room temperature. Subsequently, 850 μ l of 10 mM HCl was added dropwise and stirred for an additional 20 min to complete the hydrolysis. Finally, 2.135 ml of the azeotrope toluene/1-butanol (72.84/27.16 wt%) was added to the solution to get a concentration of 1 g ml⁻¹ of aluminosilicate. Next, the solution was filtered with a 0.2 μ m PTFE syringe filter and kept

refrigerated at 5 °C for use. Simultaneously, a BCP stock solution was prepared by dissolving 40 mg ml⁻¹ of PI-*b*-PEO in the azeotrope toluene/1-butanol.

A so-called hybrid mixture of BCP was created by combining 60 µl of the aluminosilicate stock solution with 750 µl of the BCP stock solution in a glass vial, which was then placed on a shaker for 30 min prior to use.

Thin films were prepared by spin-coating (2,000 rpm, 20 s, Laurell WS 650 MZ) 40 µl of the hybrid solution onto the substrates used for characterization and sensing. These hybrid thin films were subsequently reactive ion etched (2 min, CHF₃/Ar 15/50, 2 min, 215 W, 40 mbar, PlasmaPro 80 RIE, OXFORD instruments) to remove the upper layer of segregated aluminosilicate aiming to obtain a fully open superficial porous structure, as we have shown in a previous work with enzymes.³⁵ Samples were then calcined in argon (450 °C, 30 min, 5 °C min⁻¹) in a tubular furnace, left to cool inside the tube and later calcined in air (450 °C, 30 min, 5 °C min⁻¹).

The following substrates were used for characterization and sensing. FTO-coated glass (20 x 15 mm², TEC 6, Pilkington) was used as the working electrode for electrochemical DNA sensing. Silica-coated QCM-D sensors (5 MHz 14 mm Cr/Au/SiO₂, Quartz PRO) were used for QCM-D measurements. Silicon substrates (10 x10 mm², 1-side polished, p-type boron, MicroChemicals) were deployed for microscopy, ellipsometric and GISAXS characterization. Gold-coated silicon substrates (10 x 10 mm², Au thickness: 100 nm, coated in an Edwards E306A Bell Jar Thermal Evaporator) were used for FTIR measurements.

Immobilization of ssDNA capture probes on the nanoporous layer: Immobilization of the amino-modified capture probes (ssDNA-NH₂) in the sensors was achieved following a 5-step functionalization procedure. First, nanoporous sensors were plasma-treated in oxygen (15 s, 100 W, 0.33 mbar, Diener Electronic “Pico”) to introduce OH groups on the surface. Second, the sensor

surface was aminosilanized by immersing for 20 min in a 5% V/V solution of APTES in anhydrous toluene under an argon atmosphere and room temperature. The functionalized sensors were then sonicated two times for 5 min in toluene and then in ethanol to remove unreacted material from the surface. Third, the sensors were immersed in a solution of 10% V/V of glutaraldehyde in 0.1 M PBS buffer for 30 min at room temperature in air to attach the homobifunctional crosslinker to the amine groups. Nanoporous sensors were then rinsed and sonicated two times for 5 min in PBS to remove unreacted glutaraldehyde molecules. Fourth, modified sensors were incubated overnight at 4 °C in a 1 μM ssDNA-NH₂ in 0.1 M PBS buffer. The sensor surface was then rinsed three times with a 0.1 M PBS solution. Fifth, the remaining aldehyde groups were blocked with a mixture of 0.1 M ethanolamine and 0.1 M sodium cyanoborohydride in 0.1 M PBS buffer for 30 min. Please note that the PBS buffer used for immobilization and sensing was prepared using nuclease-free water.

Material characterization

Spectroscopic ellipsometry (SE) and ellipsometric porosimetry (EP): SE and EP measurements were recorded on nanoporous films deposited onto silicon substrates using an ellipsometer with variable angle (incident angle of 73°, spectra: 300 to 989 nm, SE-2000, Semilab). The measured Ψ and Δ spectra were fitted using the integrated SEA software (Semilab). Refractive index and film thickness were obtained from the experimental data by using a Cauchy dispersion law and Levenberg–Marquardt algorithm (LMA) with a fit quality $R^2 > 0.95$. Porosity was calculated based on variations in the refractive index resulting from toluene adsorption, utilizing the Lorentz-Lorentz effective medium approximation and a simplex fitting algorithm with a $1e^{-6}$ error tolerance and up to 1,000 iterations. The distribution of pore sizes was determined using the modified Kelvin

equation. It was assumed that the contact angle for toluene on aluminosilicate surfaces is zero, indicating complete wetting.

Grazing-incidence small-angle scattering (GISAXS): GISAXS measurements were completed in a Ganesha 300XL instrument (Xenocs SAXSLAB) on thin films deposited onto silicon substrates. A high-brilliance microfocus Cu-source ($\lambda = 1.5418 \text{ \AA}$) was used. A PILATUS 300K solid-state photon-counting detector at a sample-to-detector distance of 950 mm and an incidence angle of 0.16° served to collect 2D GISAXS scattering patterns. FitGISAXS⁶¹ software was used for GISAXS data analysis.

Atomic force microscopy (AFM): AFM images were obtained in tapping mode with a Dimension Icon Instrument (Bruker) using a Bruker ScanAsyst Air Probe with a nominal tip radius of 2 nm. The software WSXM was used for AFM image analysis.⁶²

Scanning electron microscopy: SEM images of the aluminosilicate nanoporous films were obtained in an Xbeam 540 FIB/SEM (ZEISS), using short working distance (0.9 to 1 mm) and low acceleration voltage (0.5 to 2 kV). Image analysis was performed with the software WSXM.

Focused ion beam: High magnification image of the nanoporous film surface was captured in a FIB microscope (He, acceleration voltage 25 kV, Orion Nanofab, Carl Zeiss).

Fourier Transform Infrared Spectroscopy: An infrared microscope coupled with an FTIR spectrophotometer (AIM-9000, IRTracer-1000, Shimadzu) was used to record the FTIR spectra in reflection mode on nanoporous thin films fabricated onto gold-coated silicon substrates. The software Lab Solutions IR (Shimadzu) was used to perform atmospheric and baseline corrections.

Quartz crystal microbalance: Nucleic acid immobilization and hybridization kinetics were studied with a quartz crystal microbalance (Q-Sense E4 instrument, Biolin Scientific) using flat silica-coated QCM-D sensors (5 MHz 14 mm Cr/Au/SiO₂, Quartz PRO) and nanoporous-coated

QCM-D sensors with an active area of 0.79 cm². A flow rate of 30 µl min⁻¹ was set to pump solutions into the QCM-D chamber. Frequency analysis was performed with the software QSense Dfind (Biolin Scientific).

Electrochemical detection of DNA

Electrochemical measurements: Electrochemical measurements were obtained in a three-electrode configuration using a PTFE cell containing the working electrode (0.5 cm², FTO coated glass) coated with the nanoporous film functionalized with the capture probes, a silver/silver chloride reference electrode (4 mm diameter, Gamry), and a platinum wire as a counter electrode (0.4 mm diameter, Gamry), as shown in Supporting Information **Figure S3**. EIS measurements (100 kHz to 0.1 Hz, amplitude 50 mV, 0 V vs OCP) were carried out using a potentiostat (Reference 600+, Gamry). Electrochemical measurements were analyzed and modeled using the Gamry Echem Analyst software.

Electrochemical detection protocol: The working electrodes functionalized with the capture probes (complementary and non-complementary to the target DNA) were mounted in the electrochemical cell. An initial EIS measurement was performed in 2 mM [Fe(CN)₆]^{3/4-} in PBS buffer, pH 7.4. The sensor was then rinsed with PBS, and a new EIS measurement was performed. This process was repeated until two consecutive EIS measurements were identical to ensure stability in the measurements. Then, target ssDNA in a concentration from 1 pM to 1 nM prepared in 0.1 M PBS buffer were sequentially incubated on the electrode surface for 20 min. EIS measurements were performed before and after the target ssDNA incubation. EIS measurements with complementary nucleic acid were performed with four sensors. Three sensors were measured with the non-complementary capture probe as a negative control.

Corresponding Author

E-mails: s.guldin@ucl.ac.uk, n.voelcker@monash.edu

Author Contributions

The manuscript was written through contributions of all authors. All authors have given approval to the final version of the manuscript.

Funding Sources

M.J.J.F acknowledges funding from the Swiss National Science Foundation (SNSF) through project P500PN_217951. M.J.J.F., A.A.-F., and S.G. are grateful for funding by an EPSRC New Investigator award (Award No. EP/R035105/1). This work was performed in part at the Melbourne Centre for Nanofabrication (MCN) in the Victorian Node of the Australian National Fabrication Facility (ANFF). AAR acknowledges funding from the European Union's Horizon 2020 research and innovation program under the Marie Skłodowska-Curie grant agreement No.713679.

Acknowledgments

The authors are grateful to Dr Virginie Ponsinec and Ahmed Bentaleb (Université de Bordeaux, CNRS) for support with the GISAXS measurements.

Supporting Information

Cross section of a nanoporous thin film; Surface modification QCM-D sensor using ssDNA-modified with fluorescent tags; Image and schematic of the electrochemical cell assembly; DNA hybridization time analysis; Charge transfer resistance, limit of detection and limit of quantification.

References

- (1) Udugama, B.; Kadhiresan, P.; Kozlowski, H. N.; Malekjahani, A.; Osborne, M.; Li, V. Y. C.; Chen, H.; Mubareka, S.; Gubbay, J. B.; Chan, W. C. W. Diagnosing COVID-19: The Disease and Tools for Detection. *ACS Nano* **2020**, *14* (4), 3822–3835. <https://doi.org/10.1021/acsnano.0c02624>.
- (2) Hessels, D.; Schalken, J. A. The Use of PCA3 in the Diagnosis of Prostate Cancer. *Nat Rev Urol* **2009**, *6* (5), 255–261. <https://doi.org/10.1038/nrurol.2009.40>.
- (3) Dawson, S.-J.; Tsui, D. W. Y.; Murtaza, M.; Biggs, H.; Rueda, O. M.; Chin, S.-F.; Dunning, M. J.; Gale, D.; Forshew, T.; Mahler-Araujo, B.; Rajan, S.; Humphray, S.; Becq, J.; Halsall, D.; Wallis, M.; Bentley, D.; Caldas, C.; Rosenfeld, N. Analysis of Circulating Tumor DNA to Monitor Metastatic Breast Cancer. *New England Journal of Medicine* **2013**, *368* (13), 1199–1209. <https://doi.org/10.1056/NEJMoa1213261>.
- (4) Darling, J. A.; Frederick, R. M. Nucleic Acids-Based Tools for Ballast Water Surveillance, Monitoring, and Research. *J Sea Res* **2018**, *133*, 43–52. <https://doi.org/10.1016/j.seares.2017.02.005>.
- (5) Palchetti, I.; Mascini, M. Nucleic Acid Biosensors for Environmental Pollution Monitoring. *Analyst* **2008**, *133* (7), 846–854. <https://doi.org/10.1039/b802920m>.
- (6) Ivnitski, D.; O’Neil, D. J.; Gattuso, A.; Schlicht, R.; Calidonna, M.; Fisher, R. Nucleic Acid Approaches for Detection and Identification of Biological Warfare and Infectious Disease Agents. *Biotechniques* **2003**, *35* (4), 862–869. <https://doi.org/10.2144/03354ss03>.
- (7) Yang, S.; Rothman, R. E. PCR-Based Diagnostics for Infectious Diseases: Uses, Limitations, and Future Applications in Acute-Care Settings. *Lancet Infectious Diseases* **2004**, *4* (6), 337–348. [https://doi.org/10.1016/S1473-3099\(04\)01044-8](https://doi.org/10.1016/S1473-3099(04)01044-8).

- (8) Valasek, M. A.; Repa, J. J. The Power of Real-Time PCR. *American Journal of Physiology - Advances in Physiology Education* **2005**, *29* (3), 151–159. <https://doi.org/10.1152/advan.00019.2005>.
- (9) Afzal, A. Molecular Diagnostic Technologies for COVID-19: Limitations and Challenges. *J Adv Res* **2020**, *26*, 149–159. <https://doi.org/10.1016/j.jare.2020.08.002>.
- (10) Klein, D. Quantification Using Real-Time PCR Technology: Applications and Limitations. *Trends Mol Med* **2002**, *8* (6), 257–260. [https://doi.org/10.1016/S1471-4914\(02\)02355-9](https://doi.org/10.1016/S1471-4914(02)02355-9).
- (11) Hajia, M. Limitations of Different PCR Protocols Used in Diagnostic Laboratories: A Short Review. *Modern Medical Laboratory Journal* **2018**, *1* (1), 1–6. <https://doi.org/10.30699/mmlj17-01-01>.
- (12) Santhanam, M.; Algov, I.; Alfonta, L. DNA/RNA Electrochemical Biosensing Devices a Future Replacement of PCR Methods for a Fast Epidemic Containment. *Sensors* **2020**, *20* (16), 1–15. <https://doi.org/10.3390/s20164648>.
- (13) Rajeev, G.; Prieto Simon, B.; Marsal, L. F.; Voelcker, N. H. Advances in Nanoporous Anodic Alumina-Based Biosensors to Detect Biomarkers of Clinical Significance: A Review. *Adv Healthc Mater* **2018**, *7* (5), 1700904. <https://doi.org/10.1002/adhm.201700904>.
- (14) Reta, N.; Saint, C. P.; Michelmore, A.; Prieto-Simon, B.; Voelcker, N. H. Nanostructured Electrochemical Biosensors for Label-Free Detection of Water- and Food-Borne Pathogens. *ACS Appl Mater Interfaces* **2018**, *10* (7), 6055–6072. <https://doi.org/10.1021/acsami.7b13943>.
- (15) De La Escosura-Muñiz, A.; Merkoçi, A. A Nanochannel/Nanoparticle-Based Filtering and Sensing Platform for Direct Detection of a Cancer Biomarker in Blood. *Small* **2011**, *7* (5), 675–682. <https://doi.org/10.1002/smll.201002349>.

- (16) Shiohara, A.; Wojnilowicz, M.; Lyu, Q.; Pei, Y.; Easton, C. D.; Chen, Y.; White, J. F.; McAuley, A.; Prieto-Simon, B.; Thissen, H.; Voelcker, N. H. SARS-CoV-2 Virus Detection Via a Polymeric Nanochannel-Based Electrochemical Biosensor. *Small* **2023**, *19* (51), 2205281. <https://doi.org/10.1002/SMLL.202205281>.
- (17) Vlassiouk, I.; Takmakov, P.; Smirnov, S. Sensing DNA Hybridization via Ionic Conductance through a Nanoporous Electrode. *Langmuir* **2005**, *21* (11), 4776–4778. <https://doi.org/10.1021/la0471644>.
- (18) De La Escosura-Muñiz, A.; Merkoçi, A. Label-Free Voltammetric Immunosensor Using a Nanoporous Membrane Based Platform. *Electrochem commun* **2010**, *12* (6), 859–863. <https://doi.org/10.1016/j.elecom.2010.04.007>.
- (19) Huo, Q.; Wang, K.; Xu, J.-J.; Li, J.; Li, S.-J.; Wang, C.; Chen, H.-Y.; Xia, X.-H. A Nanochannel Array-Based Electrochemical Device for Quantitative Label-Free DNA Analysis. *ACS Nano* **2010**, *4* (11), 6417–6424. <https://doi.org/10.1021/nn101050r>.
- (20) Guo, K.; Sharma, A.; Toh, R. J.; Álvarez de Eulate, E.; Gengenbach, T. R.; Cetó, X.; Voelcker, N. H.; Prieto-Simón, B. Porous Silicon Nanostructures as Effective Faradaic Electrochemical Sensing Platforms. *Adv Funct Mater* **2019**, *29* (24), 1809206. <https://doi.org/10.1002/adfm.201809206>.
- (21) Espinoza-Castañeda, M.; Escosura-Muñiz, A. de la; Chamorro, A.; Torres, C. de; Merkoçi, A. Nanochannel Array Device Operating through Prussian Blue Nanoparticles for Sensitive Label-Free Immunodetection of a Cancer Biomarker. *Biosens Bioelectron* **2015**, *67*, 107–114. <https://doi.org/10.1016/j.bios.2014.07.039>.

- (22) de la Escosura-Muñiz, A.; Chunglok, W.; Surareungchai, W.; Merkoçi, A. Nanochannels for Diagnostic of Thrombin-Related Diseases in Human Blood. *Biosens Bioelectron* **2013**, *40* (1), 24–31. <https://doi.org/10.1016/j.bios.2012.05.021>.
- (23) Reta, N.; Michelmore, A.; Saint, C.; Prieto-Simón, B.; Voelcker, N. H. Porous Silicon Membrane-Modified Electrodes for Label-Free Voltammetric Detection of MS2 Bacteriophage. *Biosens Bioelectron* **2016**, *80*, 47–53. <https://doi.org/10.1016/j.bios.2016.01.038>.
- (24) Tieu, T.; Alba, M.; Elnathan, R.; Cifuentes-Rius, A.; Voelcker, N. H. Advances in Porous Silicon-Based Nanomaterials for Diagnostic and Therapeutic Applications. *Adv Ther (Weinh)* **2019**, *2* (1), 1800095. <https://doi.org/10.1002/adtp.201800095>.
- (25) de la Escosura-Muñiz, A.; Merkoçi, A. Nanochannels for Electrical Biosensing. *TrAC - Trends in Analytical Chemistry* **2016**, *79*, 134–150. <https://doi.org/10.1016/j.trac.2015.12.003>.
- (26) Shiohara, A.; Easton, C. D.; Prieto-Simon, B.; Voelcker, N. H. Electrochemical Biosensors Based on Convectively Assembled Colloidal Crystals. *Biosensors (Basel)* **2022**, *12* (7), 480. <https://doi.org/10.3390/bios12070480>.
- (27) Lokupitiya, H. N.; Jones, A.; Reid, B.; Guldin, S.; Stefik, M. Ordered Mesoporous to Macroporous Oxides with Tunable Isomorphic Architectures: Solution Criteria for Persistent Micelle Templates. *Chemistry of Materials* **2016**, *28* (6), 1653–1667. <https://doi.org/10.1021/acs.chemmater.5b04407>.
- (28) Hench, L. L.; West, J. K. The Sol-Gel Process. *Chem Rev* **1990**, *90* (1), 33–72. <https://doi.org/10.1021/cr00099a003>.

- (29) Brinker, C. J.; Scherer, G. W. *Sol-Gel Science: The Physics and Chemistry of Sol-Gel Processing*; Elsevier Inc., 2013. <https://doi.org/10.1016/C2009-0-22386-5>.
- (30) Alvarez-Fernandez, A.; Jara Fornerod, M.; Reid, B.; Guldin, S. Solvent Vapor Annealing for Controlled Pore Expansion of Block Copolymer-Assembled Inorganic Mesoporous Films. *Langmuir* **2022**, *38* (10), 3297–3304. <https://doi.org/10.1021/acs.langmuir.2c00074>.
- (31) Reid, B.; Alvarez-Fernandez, A.; Schmidt-Hansberg, B.; Guldin, S. Tuning Pore Dimensions of Mesoporous Inorganic Films by Homopolymer Swelling. *Langmuir* **2019**, *35* (43), 14074–14082. <https://doi.org/10.1021/acs.langmuir.9b03059>.
- (32) Sarkar, A.; Thyagarajan, A.; Cole, A.; Stefik, M. Widely Tunable Persistent Micelle Templates: Via Homopolymer Swelling. *Soft Matter* **2019**, *15* (26), 5193–5203. <https://doi.org/10.1039/c9sm00484j>.
- (33) Alvarez-Fernandez, A.; Reid, B.; Suthar, J.; Choy, S. Y.; Jara Fornerod, M.; Mac Fhionnlaioich, N.; Yang, L.; Schmidt-Hansberg, B.; Guldin, S. Fractionation of Block Copolymers for Pore Size Control and Reduced Dispersity in Mesoporous Inorganic Thin Films. *Nanoscale* **2020**, *12* (35), 18455–18462. <https://doi.org/10.1039/d0nr05132b>.
- (34) Jara Fornerod, M. J.; Alvarez-Fernandez, A.; Williams, E. R.; Skoda, M. W. A.; Prieto-Simon, B.; Voelcker, N. H.; Stefik, M.; Coppens, M. O.; Guldin, S. Enhanced Structural Control of Soft-Templated Mesoporous Inorganic Thin Films by Inert Processing Conditions. *ACS Appl Mater Interfaces* **2022**, *14* (50), 56143–56155. <https://doi.org/10.1021/acsami.2c18090>.
- (35) Jara Fornerod, M. J.; Alvarez-Fernandez, A.; Michalska, M.; Papakonstantinou, I.; Guldin, S. Glucose Oxidase Loading in Ordered Porous Aluminosilicates: Exploring the Potential

- of Surface Modification for Electrochemical Glucose Sensing. *Chemistry of Materials* **2023**, *35* (18), 7577–7587. <https://doi.org/10.1021/acs.chemmater.3c01202>.
- (36) Etienne, M.; Quach, A.; Grosso, D.; Nicole, L.; Sanchez, C.; Walcarius, A. Molecular Transport into Mesostructured Silica Thin Films: Electrochemical Monitoring and Comparison between P6m, P63//WWIC, and Pm3n Structures. *Chemistry of Materials* **2007**, *19* (4), 844–856. <https://doi.org/10.1021/cm0625068>.
- (37) Steinberg, P. Y.; Zanotto, F. M.; Soler-Illia, G. J. A. A.; Dassie, S. A.; Angelomé, P. C. Molecular Transport through TiO₂ Mesoporous Thin Films: Correlation with the Partially Blocked Electrode Model. *Journal of Physical Chemistry C* **2021**, *125* (42), 23521–23532. <https://doi.org/10.1021/acs.jpcc.1c07512>.
- (38) Thommes, M.; Kaneko, K.; Neimark, A. V.; Olivier, J. P.; Rodriguez-Reinoso, F.; Rouquerol, J.; Sing, K. S. W. Physisorption of Gases, with Special Reference to the Evaluation of Surface Area and Pore Size Distribution (IUPAC Technical Report). *Pure and Applied Chemistry* **2015**, *87* (9–10), 1051–1069. <https://doi.org/10.1515/pac-2014-1117>.
- (39) Baklanov, M. R.; Mogilnikov, K. P.; Polovinkin, V. G.; Dultsev, F. N. Determination of Pore Size Distribution in Thin Films by Ellipsometric Porosimetry. *Journal of Vacuum Science & Technology B: Microelectronics and Nanometer Structures* **2000**, *18* (3), 1385. <https://doi.org/10.1116/1.591390>.
- (40) Alvarez-Fernandez, A.; Reid, B.; Jara Fornerod, M.; Taylor, A.; Divitini, G.; Guldin, S. Structural Characterization of Mesoporous Thin Film Architectures: A Tutorial Overview. *ACS Appl Mater Interfaces* **2020**, *12* (5), 5195–5208. <https://doi.org/10.1021/acsami.9b17899>.

- (41) Hamley, I. W.; Castelletto, V. Small-Angle Scattering of Block Copolymers in the Melt, Solution and Crystal States. *Progress in Polymer Science (Oxford)* **2004**, *29* (9), 909–948. <https://doi.org/10.1016/j.progpolymsci.2004.06.001>.
- (42) Du, P.; Li, M.; Douki, K.; Li, X.; Garcia, C. B. W.; Jain, A.; Smilgies, D. M.; Fetters, L. J.; Gruner, S. M.; Wiesner, U.; Ober, C. K. Additive-Driven Phase-Selective Chemistry in Block Copolymer Thin Films: The Convergence of Top-down and Bottom-up Approaches. *Advanced Materials* **2004**, *16* (12), 953–957. <https://doi.org/10.1002/adma.200306189>.
- (43) Guo, K.; Alba, M.; Chin, G. P.; Tong, Z.; Guan, B.; Sailor, M. J.; Voelcker, N. H.; Prieto-Simón, B. Designing Electrochemical Biosensing Platforms Using Layered Carbon-Stabilized Porous Silicon Nanostructures. *ACS Appl Mater Interfaces* **2022**, *14* (13), 15565–15575. <https://doi.org/10.1021/acsami.2c02113>.
- (44) Kant, K.; Yu, J.; Priest, C.; Shapter, J. G.; Losic, D. Impedance Nanopore Biosensor: Influence of Pore Dimensions on Biosensing Performance. *Analyst* **2014**, *139* (5), 1134–1140. <https://doi.org/10.1039/c3an01933k>.
- (45) Devarakonda, S.; Ganapathysubramanian, B.; Shrotriya, P. Impedance-Based Nanoporous Anodized Alumina/ITO Platforms for Label-Free Biosensors. *ACS Appl Mater Interfaces* **2022**, *14* (1), 150–158. <https://doi.org/10.1021/acsami.1c17243>.
- (46) Dorfman, K. D.; Gupta, D.; Jain, A.; Muralidhar, A.; Tree, D. R. Hydrodynamics of DNA Confined in Nanoslits and Nanochannels. *The European Physical Journal Special Topics* **2014**, *223* (14), 3179–3200. <https://doi.org/10.1140/EPJST/E2014-02326-4>.
- (47) Dorfman, K. D. The Statistical Segment Length of DNA: Opportunities for Biomechanical Modeling in Polymer Physics and Next-Generation Genomics. *J Biomech Eng* **2018**, *140* (2). <https://doi.org/10.1115/1.4037790>.

- (48) Gooding, J. J. Electrochemical DNA Hybridization Biosensors. *Electroanalysis* **2002**, *14* (17), 1149–1156. [https://doi.org/10.1002/1521-4109\(200209\)14:17<1149::AID-ELAN1149>3.0.CO;2-8](https://doi.org/10.1002/1521-4109(200209)14:17<1149::AID-ELAN1149>3.0.CO;2-8).
- (49) Lin, C. H.; Hung, C. H.; Hsiao, C. Y.; Lin, H. C.; Ko, F. H.; Yang, Y. S. Poly-Silicon Nanowire Field-Effect Transistor for Ultrasensitive and Label-Free Detection of Pathogenic Avian Influenza DNA. *Biosens Bioelectron* **2009**, *24* (10), 3019–3024. <https://doi.org/10.1016/j.bios.2009.03.014>.
- (50) Rodahl, M.; Höök, F.; Fredriksson, C.; Keller, C. A.; Krozer, A.; Brzezinski, P.; Voinova, M.; Kasemo, B. Simultaneous Frequency and Dissipation Factor QCM Measurements of Biomolecular Adsorption and Cell Adhesion. *Faraday Discuss* **1997**, *107*, 229–246. <https://doi.org/10.1039/a703137h>.
- (51) Majoul, N.; Aouida, S.; Bessaïs, B. Progress of Porous Silicon APTES-Functionalization by FTIR Investigations. *Appl Surf Sci* **2015**, *331*, 388–391. <https://doi.org/10.1016/j.apsusc.2015.01.107>.
- (52) Hiraoui, M.; Guendouz, M.; Lorrain, N.; Moadhen, A.; Haji, L.; Oueslati, M. Spectroscopy Studies of Functionalized Oxidized Porous Silicon Surface for Biosensing Applications. *Mater Chem Phys* **2011**, *128* (1–2), 151–156. <https://doi.org/10.1016/j.matchemphys.2011.02.052>.
- (53) Froehlich, E.; Mandeville, J. S.; Weinert, C. M.; Kreplak, L.; Tajmir-Riahi, H. A. Bundling and Aggregation of DNA by Cationic Dendrimers. *Biomacromolecules* **2011**, *12* (2), 511–517. <https://doi.org/10.1021/bm1013102>.
- (54) Srinivasan, R.; Karaoz, U.; Volegova, M.; MacKichan, J.; Kato-Maeda, M.; Miller, S.; Nadarajan, R.; Brodie, E. L.; Lynch, S. V. Use of 16S RRNA Gene for Identification of a

- Broad Range of Clinically Relevant Bacterial Pathogens. *PLoS One* **2015**, *10* (2), e0117617. <https://doi.org/10.1371/JOURNAL.PONE.0117617>.
- (55) Lisdat, F.; Schäfer, D. The Use of Electrochemical Impedance Spectroscopy for Biosensing. *Anal Bioanal Chem* **2008**, *391* (5), 1555–1567. <https://doi.org/10.1007/s00216-008-1970-7>.
- (56) Lavín, Á.; de Vicente, J.; Holgado, M.; Laguna, M. F.; Casquel, R.; Santamaría, B.; Maigler, M. V.; Hernández, A. L.; Ramírez, Y. On the Determination of Uncertainty and Limit of Detection in Label-Free Biosensors. *Sensors* **2018**, *18* (7), 2038. <https://doi.org/10.3390/s18072038>.
- (57) Chin, G. P.; Guo, K.; Vasani, R.; Voelcker, N. H.; Prieto-Simón, B. Carbon-Stabilized Porous Silicon Biosensor for the Ultrasensitive Label-Free Electrochemical Detection of Bacterial RNA Gene Fragments. *Biosens Bioelectron X* **2024**, *16*, 100438. <https://doi.org/10.1016/J.BIOSX.2024.100438>.
- (58) Forootan, A.; Sjöback, R.; Björkman, J.; Sjögreen, B.; Linz, L.; Kubista, M. Methods to Determine Limit of Detection and Limit of Quantification in Quantitative Real-Time PCR (QPCR). *Biomol Detect Quantif* **2017**, *12*, 1–6. <https://doi.org/10.1016/j.bdq.2017.04.001>.
- (59) Zorn, M. E.; Gibbons, R. D.; Sonzogni, W. C. Evaluation of Approximate Methods for Calculating the Limit of Detection and Limit of Quantification. *Environ Sci Technol* **1999**, *33* (13), 2291–2295. <https://doi.org/10.1021/es981133b>.
- (60) Zhou, X.; Schuh, D. A.; Castle, L. M.; Furst, A. L. Recent Advances in Signal Amplification to Improve Electrochemical Biosensing for Infectious Diseases. *Front Chem* **2022**, *10*, 614. <https://doi.org/10.3389/fchem.2022.911678>.

- (61) Babonneau, D. FitGISAXS: Software Package for Modelling and Analysis of GISAXS Data Using IGOR Pro. *J Appl Crystallogr* **2010**, *43* (4), 929–936. <https://doi.org/10.1107/S0021889810020352>.
- (62) Horcas, I.; Fernández, R.; Gómez-Rodríguez, J. M.; Colchero, J.; Gómez-Herrero, J.; Baro, A. M. WSXM: A Software for Scanning Probe Microscopy and a Tool for Nanotechnology. *Review of Scientific Instruments* **2007**, *78* (1), 013705. <https://doi.org/10.1063/1.2432410>.